Low cost external serial interface watchdog for SoCs and FPGAs automatic characterization tests

Numerical Investigation of the Performance of a Solar Air Heater Equipped with Packed Beds

Hossein Ebadi[1], Antonio Cammi[2], Laura Savoldi[1]

[1] MAHTEP Group, Dipartimento Energia "Galileo Ferraris" (DENERG), Politecnico di Torino, Italy
[2] Department of Energy, Politecnico di Milano, Italy

Abstract

In this work, a numerical study based on pore-scale CFD analysis has been carried out on a solar air heater equipped with intermittent packed beds. Hydraulic and thermal characteristics of the air were determined by testing a range of mass flow rates and various collector configurations, including one (SAH-M1), two (SAH-M2), and three (SAH-M3) packed beds. After the validation of the numerical simulations with general correlations, results showed that as the number of packed zones increases, the total pressure drop grows. As a result, the maximum pressure drop was obtained as 115 kPa for the collector with three packed zones, operating at $Re \sim 1.3 \times 10^5$. Detailed thermal analysis proved that the intermittent integration of packed beds has the potential to also increase the heat transfer exchange between each packed zone, improving the convection by 25% in the second zone to the first zone and 35% in the third zone to the second zone at $Re \sim 1.3 \times 10^5$. This enhancement effect can be attributed to the increase in the turbulence conditions of the fluid regime from one bed to the other. Evaluating the effects of design parameters showed that the bed spacing could not change the thermo-hydraulic characteristics significantly, while particles' randomness may only affect the pressure drop by 13%.

Keywords: Solar air heater, Packed bed, heat transfer coefficient, porous, PCM

1. Introduction

Solar Flat Plate Collectors (FPC) are the most mature technology cases among all the other solar collectors, which have wide dissemination in both industrial and domestic applications. In general, the sample design of such collectors has a limited efficiency, which can be extended only if any other enhancement method is employed. To this achieve aim, in addition to optical augmentation, scientists have proposed various techniques to improve the nominal thermal efficiency of FPC which can be classified as passive or active solutions (Gorjian et al., 2020).

Solar Air Heaters (SAH) is one of the low-temperature solar collectors, which has wide deployment in agricultural and residential applications. According to the reports in the literature, the integration of pack beds, usually in the form of heat storage units could increase the nominal thermal efficiency further by storing the excessive heat with sensible or latent heat energy storage systems (Kumar and Kim, 2017). In general, packed bed SAHs can be formed using a metal screen, porous matrix, or packed particles to improve the heat transfer from the absorber to fluid flow. There are numerous studies that address the application of packed beds with SAH, investigating the shape, orientation, and size of the particles used in the medium. However, most of the reported works are usually experimental (Singh et al., 2013) or have a macro-scale numerical approach (Choudhury et al., 1995) due to the complexity of the simulation of packed-bed geometry. The employment of wire mesh packed beds with solar air collectors showed an 80% higher efficiency for a double pass flow. A finite difference solution algorithm was proposed using C++ language for a two-dimensional fully-developed fluid flow to predict the heat transfer coefficient for packed bed systems (Chouksey and Sharma, 2016). In an experimental study, researchers (Prasad et al., 2009) determined the heat transfer and friction characteristics of a packed bed solar air heater using wire mesh as packing material. It was found that the friction factor is a function of the system (geometrical) and operating parameters while the mass flow rate and the porosity of the bed are two important factors affecting the thermal efficiency. An analytical model was developed by scientists (Dhiman et al., 2011) to study a parallel flow solar air heater with packed material through an iterative solution procedure solving the governing energy balance equations. Results indicated that the air mass flow rate has the highest effect on the thermal efficiency of the heater where the maximum thermal efficiency increase was 20% due to the presence of the packed material. The integration of limestone and gravel as the packed-bed material with solar air heaters was also investigated both

Selection and/or peer review under responsibility of Scientific Committee
doi:10.18086/eurosun.2022.12.05 Available at http://proceedings.ises.org

numerically and experimentally (Ramadan et al., 2007). Using an analytical solution of the energy-balance equations for the various elements of the system, researchers studied the effect of different operational and configurational parameters such as mass flow rate, and packed porosity on the heater performance and reported that the best performance could be achieved by materials with higher masses and lower porosities. In another attempt (Raj et al., 2019), phase change materials (PCM) were added to a solar air heater used for drying applications to extend the operating hour of the system after sunset. Therefore, several discrete metallic rectangular and cylindrical macro-encapsulate PCM units were placed inside the channel. Conducting a series of experimental tests, it was revealed that the average encapsulate efficiency can be obtained as 47.2% and 67% respectively for rectangular and cylindrical macro-encapsulates.

To open a new door in this field of research, this study aims to present a micro-scale (pore-scale) numerical analysis of a rectangular SAH duct equipped with packed bed inserts made by cylindrical particles with 3D CFD simulation using the commercial software of STAR CCM+. To reach this aim, the Discrete Element Method (DEM) was used to develop the geometry of the packed bed consisting of mm-size cylindrical particles. The credibility of this methodology for the development of porous structures with random packings has been well demonstrated in the literature (Allio et al., 2020; Savoldi et al., 2020). The beneficial effects in the augmentation of the heat transfer are specifically addressed in the analysis, with an eye on the increase of pressure drop driven by the presence of the packed bed inserts.

2. Solar collector

A typical SAH with dimensions of 726 mm × 80 mm × 30 mm was modeled, considering the solar absorber located over a rectangular duct, including running air. Since this study aims to model the inserts in the air channel and has no obligation to solve the energy equation on the collector's cover, the solution domain does not concern the heat transfers from the glass cover and the isolating materials. Therefore, the main emphasis of the current work is to study the behavior of the turbulent regime formed when the air passes through the packed medium. As known that the integration of packed beds will bring some pumping penalty due to the pressure drop within the medium, the proposed packed bed was designed as intermittent in three different zones as depicted in Figure 1 to reduce the expected pressure drop. The bed elements were cylinders with 10 mm diameter and 10 mm height to present the Phase Change Material (PCM) containers when heat storage materials are employed.

Each packed zone was simulated by a length of 42 mm consisting of 60 random cylinders as shown in Fig.1. The formation of the packed bed was achieved using DEM simulation, following the procedure introduced in the literature (Allio et al., 2020). This process was conducted in three stages, in which firstly, a container as the bulk volume of the matrix was devised and particles with the given dimensions were injected along the gravity to fill the container. The transient DEM simulation was continued until the number of particles reached the desired value of the target porosity, which for the case at hand, is 52 %. In the next step, particles were replaced with solid cylinders to form the packed matrix. Thus, the solid domain was built by combining the particles' geometries and their contact points with the channel structure, where the heat flux functions were applied to this domain as a boundary condition at the outer wall. Simulations were performed first for a smooth SAH and then the packed bed SAH with three configurations, investigating the hydraulic and thermal behaviors of the air inside the collector. The model SAH-M1 was developed with a solar heater equipped with a 42-mm-long packed bed, located as shown in Figure 1. The model SAH-M2 accounted for 2 packed beds with a 200 mm interval, and the model SAH-M3 was created with 3 packed beds, each 200 mm apart from the others. Thus, simulations were aimed to compare the effects of mass flow rate $\dot{m}$ (0.01, 0.05, 0.08 kg/s) on each of the proposed designs and understand how fluid behaves as it passes through each model. As far as the heat transfer coefficient is concerned, thermal modeling was added to the simulations investigating the convective heat transfer coefficients for a constant wall temperature of particles.

In this regard, the average heat transfer coefficient (h) between the fluid and solid rings was determined through the microscopic study and applying a constant wall temperature boundary condition to the cylinders. The intention of this investigation was to assess the air convective heat coefficient over the particles (PCM containers) representing a constant melting temperature. Therefore, a constant wall temperature of 600K was applied to the wall of the particles. The definition of the overall heat transfer coefficient is given in Eq.1.

$$h = \frac{\dot{m} C_p (T_o - T_i)}{S_S \, (T_s - T_m)} \qquad \text{(eq.1)}$$

where T_{mo} and T_{mi} are the mean outlet and inlet bulk temperatures of fluid Computed at the inlet/outlet of the PB zones, while ΔT_{lm} indicates the log mean temperature difference, $\boldsymbol{c_p}$ is the air specific heat, evaluated at the temperature T_m, and $\boldsymbol{S_S}$ is the total particle surface.

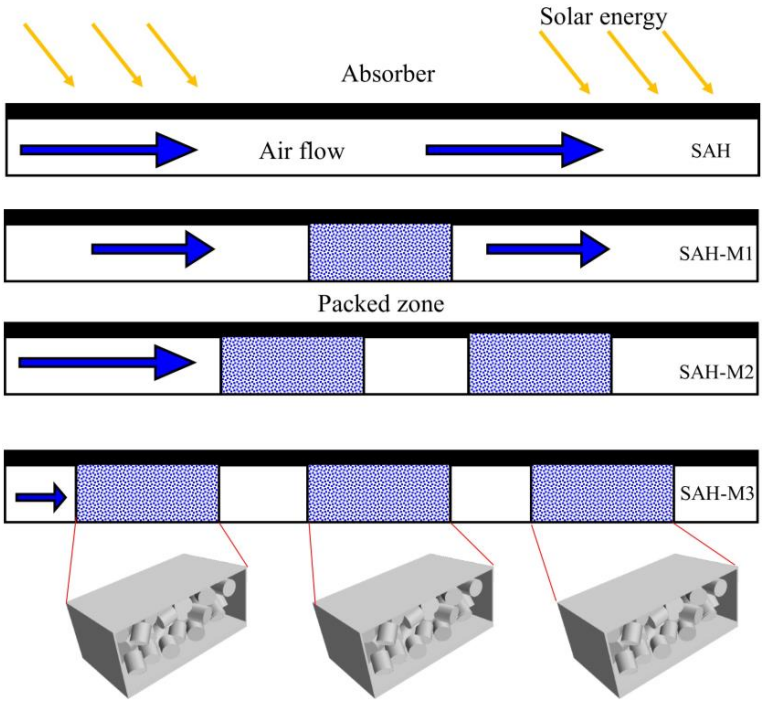

Fig. 1: Schematic of the different solar collectors equipped packed beds consisting of cylinders.

As the temperature is not uniform across the inlet and outlet cross-sectional areas, the mean inlet and out temperatures are determined using Eq.2.

$$\boldsymbol{T_m} = \frac{\int_A \boldsymbol{\rho v C_p T dA_c}}{\boldsymbol{\dot{m} C_p}} \quad \text{(eq.2)}$$

where $\boldsymbol{\rho}$ is the fluid density and v represents the fluid velocity, while the log mean temperature difference can be expressed as Eq. 3.

$$\Delta \boldsymbol{T_{lm}} \equiv \frac{(\boldsymbol{T_s - T_{mo}}) - (\boldsymbol{T_s - T_{mi}})}{\boldsymbol{ln}((\boldsymbol{T_s - T_{mo}})/(\boldsymbol{T_s - T_{mi}}))} \quad \text{(eq.3)}$$

3. Model setup

A 3D conjugate heat transfer model was selected for a steady-state condition. In order to simulate a turbulent flow inside the receiver, a two-equations Reynolds-Averaged Navier-Stokes (RANS) model, namely the two-layer realizable $k-\varepsilon$ model, was used, with a two-layer wall treatment at the wall. It is worth mentioning that $k-\varepsilon$ turbulence model is widely used in the modelling of solar tubular absorbers enhanced with inserts (Bellos et al., 2017; Bellos and Tzivanidis, 2018; Kumar and Reddy, 2020; Mwesigye et al., 2014; Yılmaz et al., 2020). The two-layer version of the $k-\varepsilon$ model adds flexibility to the wall treatment switching automatically between low-y+ and high-y+ treatments. As indicated by literature (Dixon et al., 2012), the superiority of the realizable $k-\varepsilon$ over the standard $k-\varepsilon$ model refers to the addition of an improved equation for the turbulent energy dissipation rate ε, with a variable viscosity coefficient Cμ instead of a constant value. Thus, as long as rotation boundary layers under strong adverse pressure gradients, separation, and recirculation with strong curvature are considered, similar to those found in packed tube simulation (Dong et al., 2017; Moghaddam et al., 2021), this model could result in a reasonable performance. According to the realizable $k-\varepsilon$ model, the transport equations for the turbulent kinetic energy k and for its dissipation rate ε are expressed as follows.

$$\frac{\partial}{\partial t}(\rho\kappa) + \frac{\partial}{\partial x_j}(\rho\kappa u_j) = \frac{\partial}{\partial x_j}\left[\left(\mu + \frac{\mu_t}{\sigma_\kappa}\right)\frac{\partial \kappa}{\partial x_j}\right] + G_\kappa + G_b - \rho\varepsilon - Y_M + S_\kappa \quad \text{(eq.4)}$$

$$\frac{\partial}{\partial t}(\rho\varepsilon) + \frac{\partial}{\partial x_j}(\rho\varepsilon u_j) = \frac{\partial}{\partial x_j}\left[\left(\mu + \frac{\mu_t}{\sigma_\varepsilon}\right)\frac{\partial \varepsilon}{\partial x_j}\right] + \rho C_1 S\varepsilon - \rho C_2 \frac{\varepsilon^2}{k+\sqrt{v\varepsilon}} + C_{1\varepsilon}\frac{\varepsilon}{k}C_{3\varepsilon}G_b + S_\varepsilon \quad \text{(eq.5)}$$

where G_κ and G_b refer to the kinetic energy based on mean velocity gradients and buoyancy, respectively, Y_M represents the fluctuating dilatation in compressible turbulence to the overall dissipation rate, σ_κ and σ_ε are the turbulent Prandtl numbers for the turbulent kinetic energy and its dissipation and S_κ and S_ε are source terms. Also, the eddy viscosity μ_t can be determined by Eq. 6.

$$\mu_t = \rho C_\mu \frac{\kappa^2}{\varepsilon} \quad \text{(eq.6)}$$

In the realizable $k-\varepsilon$ model, first introduced by Shih et al. (Shih et al., 1995), C_μ is a function of mean strain and rotation rates, the angular velocity of the system rotation, and the turbulence fields (k and ε) (Soe and Khaing, 2017).

The thermal analysis in this work was performed using a segregated flow temperature model and the boundary condition of a constant inlet temperature of the fluid. Since this study considers various absorber designs, a range of different boundary conditions corresponding to the flow configuration was applied in the CFD simulation as follows:

- In the case of SAH-M designs, two inlet faces were defined as mass flow inlet conditions while a pressure outlet was applied to the outlet face. In the thermal simulations, the interface between the solid and fluid domain in the packed zone was treated with a constant wall temperature to achieve the HTC in the packed zone. The collector walls were set as the adiabatic boundary conditions, while the united walls of the particles were treated with the constant wall temperature boundary conditions.
- For the validation study, a reference pressure of 1 bar was set for the simulations, while in the rest of the simulations a reference pressure of 10 bar was used to ensure the one-direction flow over the packed particles.
- To exclude the inlet effects of the running air the inlet section was elongated to a distance, which led the fluid regime to reach the necessary hydraulic characteristics related to fully developed conditions.

A polyhedral-based meshing with prismatic layers for fluid regions was employed to solve the equations. Grids were developed using a hybrid approach employing both structured and unstructured mesh. As shown in Figure 2, several custom controls were adopted to the boundary layer areas to refine the meshing with specific care, especially for the packed-bed zones where the particles are located. While in the areas, where the velocity and temperature gradients are smoother, cells become coarser and uniform along the length of the channel.

4. Validation study

An important step in the analysis of the thermal and hydraulic performance of solar air heaters is to obtain the friction factor in adiabatic conditions, which is defined through the Darcy relation (Eq. 7) for every flow. In the case of smooth SAH, a correlation is given in Eq. 8 (Azad et al., 2021).

$$f = \frac{2}{L/D_h}\frac{\Delta P}{\rho \bar{v}^2} \quad \text{(eq.7)}$$

$$f_S = 0.085 \times Re^{-0.25} \quad \text{(eq.8)}$$

where L is the length of the absorber, D_h is the hydraulic diameter of the rectangular channel, defined as $\frac{2ab}{a+b}$ in which a and b are the height and width of the channel, and v is the average inlet velocity of the air, ρ is the average density of the air, and ΔP is the pressure drop obtained through CFD simulation.

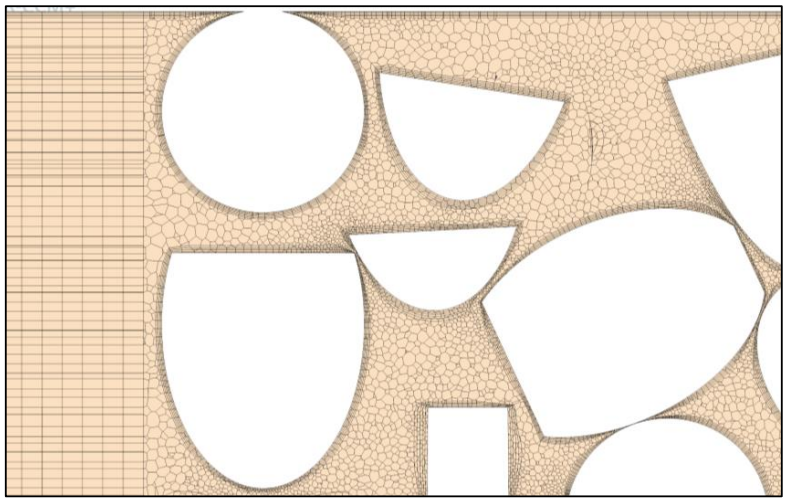

Fig. 2: Hybrid mesh used to develop the network grid for SAH-M models.

For the sake of validation in terms of Nusselt number, a smooth SAH with a constant heat load of 1000 W/m^2 was simulated and results were validated with those obtained by the Dittus-Boelter correlation as follows (Bensaci et al., 2020);

$$Nu = \frac{h \times D_h}{k} = 0.023 \times Re^{0.8} \times Pr^{0.4} \quad \text{(eq.9)}$$

$$Re = \frac{4 \times \dot{m}}{\pi D_{ri} \mu} \quad \text{(eq.10)}$$

$$Pr = \frac{\mu Cp}{k} \quad \text{(eq.11)}$$

where k is the thermal conductivity of the air computed at the average temperature T_m, and μ is the dynamic viscosity of the air. Therefore, the boundary conditions in this simulation consist of a mass flow inlet at the inlet face, and a pressure outlet at the outlet face, while a uniform heat flux was applied to the top surface of the solid plate, and an interface was defined between the fluid and solid regions.

As mentioned above, the validation process was carried out by comparing both the Nusselt number and friction factor for a range of Re numbers to check the viability of the simulation in the smooth model. According to Fig. 3a, the computation of f shows a very good agreement between the results of CFD and correlation with less than 15% error. Furthermore, as shown in Fig.3a the comparison between the values of the Nu number predicted from the correlation and those obtained with CFD simulation indicates that the discrepancy could not exceed 20%, which asserts that the current numerical procedure can capture the physics of the SAH under study.

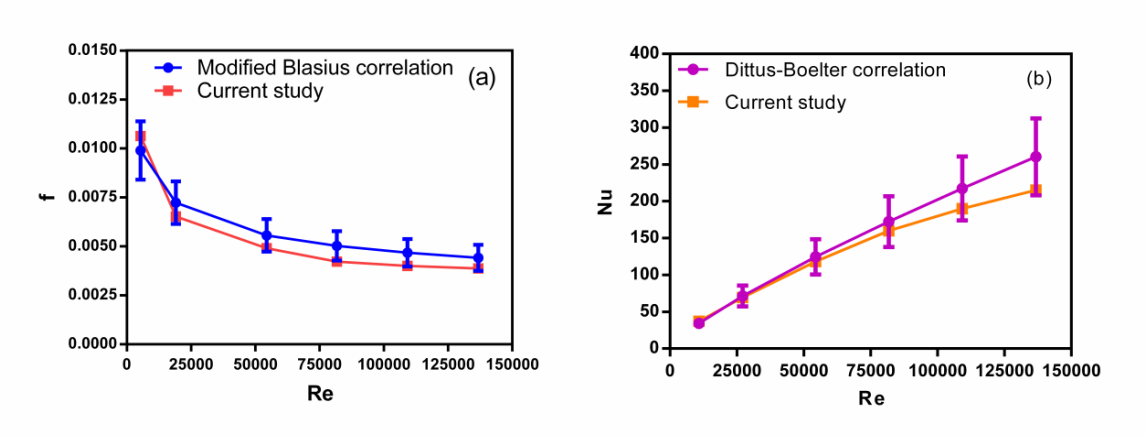

Fig. 3: Validation results: the comparison of (a) friction factor and (b) Nu number with respect to various Reynolds number.

Then to check the accuracy of the meshing grid, ensuring that results are independent of the number of cells, several cases were studied with a range of cell numbers, and the global results in terms of friction factor and Nu number were compared. The refinement of the grid has been achieved by first giving a constant base cell size and increasing the base cell size until y+ reached 1. Then, the number of prism layers was frozen, and the base cell

size was decreased until convergence was achieved in the results. Following the discussed procedure, the optimum meshes were obtained as 0.1, 17.5, 26.4, and 32.7 million cells respectively for smooth, SAH-M1, SAH-M2, and SAH-M3 models. It must be added that since y+ values were achieved as ~1 at the wall and knowing that the Prandtl number for air is close to 1, good modeling of the fluid-dynamic boundary layer (friction factor) should allow good modeling of the thermal boundary layer.

5. Results and discussion

In this section, the hydraulic performance of the proposed solar heaters is presented and flow characteristics are determined. Fig.4a shows the total pressure drops achieved through the developed models for a range of Re numbers. As shown, pressure drop increases with growth in Re number, and also increasing the number of packed beds. In more detail, when two packed beds are employed, the pressure drop increases by 100%, and when three packed beds are considered the pressure drop increases by 200% compared to the one packed bed employment. As a result, the maximum pressure drop is recorded as 115 kPa for SAH-M3 and Re ~ 1.3×10^5, and the minimum is 570 Pa in SAH-M1 and Re ~ 8×10^4. Fig.4b provides the detailed pressure drops computed over each packed bed in the model SAH-M3. As expected, in all the mass flow rates, the pressure drop increases from the first (PB1) to the second packed bed (PB2) due to the mixing induced by the presence PB1. However, this trend undergoes a very slight drop coming from PB2 to PB3.

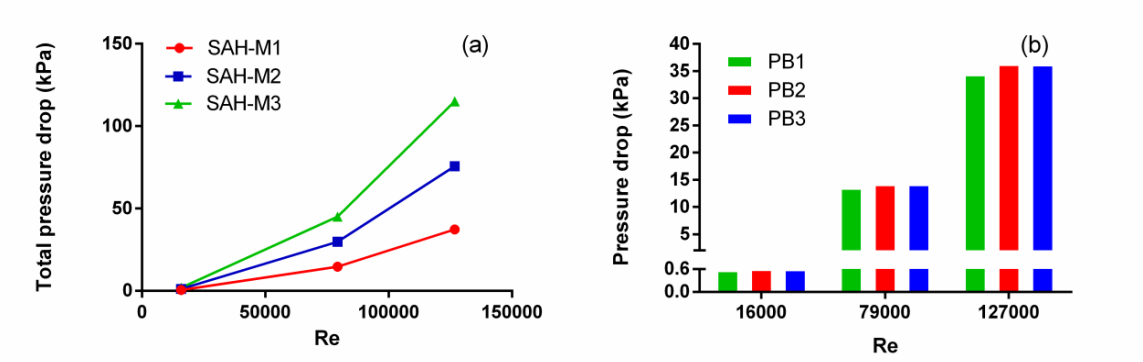

Fig. 4: (a) Total pressure drop computed for the different packed bed designs as a function of the Reynolds number; (b) pressure loss at the different porous inserts in the SAH-M3 configuration, for different values of the Reynolds number.

Fig.5 shows the air velocity counters over the first packed zones of the model SAH-M3 (Re ~ 1.6×10^4) on a cross-section along the flow axis. As shown, air attacks the first packed bed (PB1) in a fully-developed condition with no chaos in the flow. Passing through the particles, the flow boundary layers are broken, forming high-velocity contours in the narrow passages and some stagnation points where the flow passage is blocked. As a result, the air leaving the packed zone undergoes a higher turbulent condition. As observed, the particles' orientation is a factor, which affects the velocity contours formation inside the packed zone. Thus, loose packing spots can provide enough space for vortex and high-speed flow formations, while stagnation zones can be observed whiten the dense packing areas. Results follow the conclusions derived in other works (Ebadi et al., 2021).

Fig.6 represents the values of averaged air turbulent kinetic energy (TKE) obtained at the inlet of each packed bed. Results show that as the Re number increases, the value TKE grows, in view of the turbulent mixing of the flow downstream of the pebble bed, shown in Fig 5. A higher level of turbulent kinetic energy determines a higher pressure drop, as shown in Fig. 4b. Note, however, that the actual amount of the computed TKE increase is related to the distance among the PB: the smaller the distance, the higher the TKE. The distance among the PB can then become an optimization parameter to find a suitable trade-off between the increase of efficiency due to the turbulent mixing and the increase of the pressure drop.

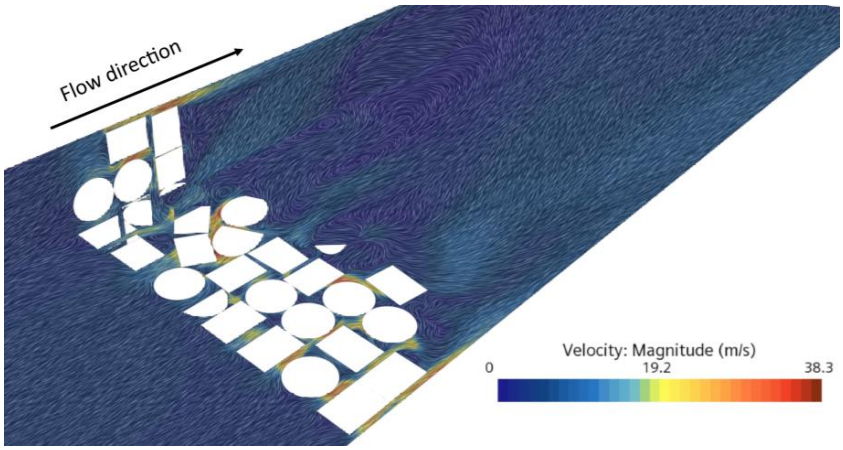

Fig. 5: Velocity field of the fluid passing through the first packed bed in the model SAH-M3 and Re ~ 16000.

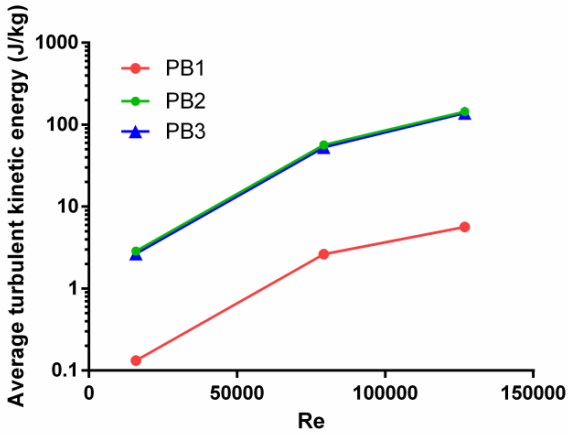

Fig. 6: The computed average turbulent kinetic energy at the inlet of each packed bed in SAH-M3 model.

Following the analysis of the flow field, an evaluation has been performed to obtain the heat transfer coefficients on various SAH designs with respect to a range of Re numbers. Figure 7 renders the air temperature profile computed along the flow direction as it passes through the first, second, and third packed zones in the model SAH-M3 and Re ~ 1.3×10^5. As shown, the random positioning of the particles plays an important role in forming the temperature contours, where those located perpendicular to the flow have a higher contribution to the air temperature increase, while others aligned with the flow direction lead to lower heat exchange.

Fig.8a illustrates the various convective heat coefficients obtained on each packed bed, respecting various Re numbers. As expected, increasing the turbulence inside the fluid regime improves the amount of heat transferred to the fluid where the maximum convective heat coefficients are obtained at Re ~ 1.3×10^5. Moreover, when the flowing air passes through the first packed bed, undergoes a sudden increase in its TKE, which improves its ability to convey the heat to the next packed bed. Furthermore, when the air reaches the third packed bed, h enhances further, hitting its maximum value under three mass flow rates. According to Fig. 8b, a comparison has been made to assess the increments in convective heat coefficients computed along each packed bed. As shown, for the low and medium mass flow rates, the increase in heat convection between the second and first packed beds is higher than that measured among the third and second packed beds. When the air mass flow rates increase to the highest value (Re ~ 1.3×10^5), the comparison results become reversed, putting the h_{PB3}/h_{PB2} ratio higher than h_{PB2}/h_{PB1}. Thus, a 25% enhancement is obtained by comparing the values of h for PB2 to those of PB1 at Re ~ 1.3×10^5. While this convection improvement continues to rise, reaching the third packed zone with a nearly 35% increase compared to PB2. As a result, the intermittent implementation of packed zones has positively affected the heat transfer improvement, increasing the turbulence conditions in the fluid regime from one bed to the other.

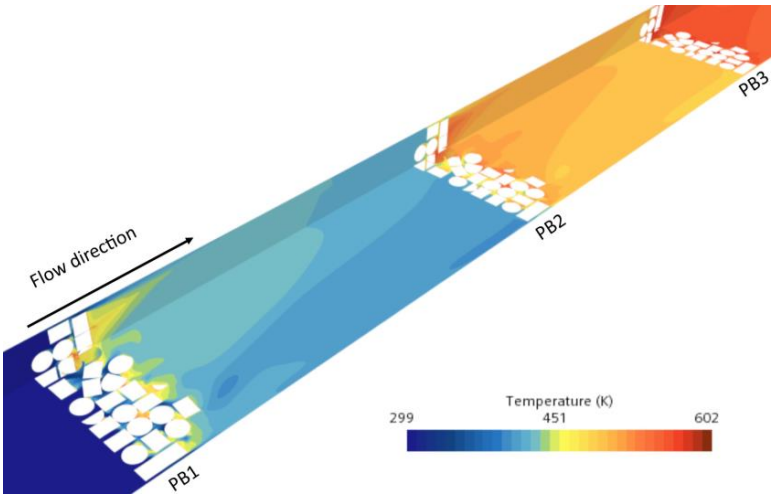

Fig. 7: Temperature map obtained for the fluid passes through each bed in the model SAH-M3 and Re ~ 127000.

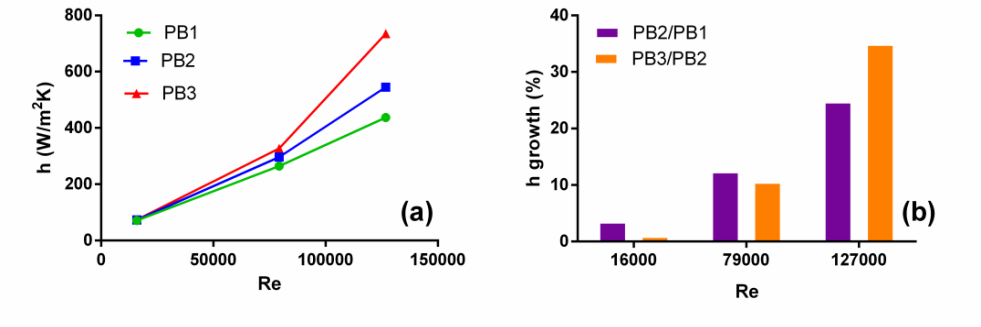

Fig. 8: (a) The convective heat transfer coefficients obtained on each packed bed in the model SAH-M3, (b) the change ratio among each packed bed.

In this section, a comparison study has been carried out to assess the effects of particle randomness and bed spacing on the hydrothermal performance of the collector with three packed beds (SAH-M3). Therefore, a number of simulations were used, where first, the flow direction is reversed compared to the default investigations to take into account the randomness parameter. Then two more configurations with different packed bed spacing, including 150 and 100 mm length were developed to find the deviations in the values of pressure drop and heat convection coefficient compared to 200 mm length. According to Fig. 9, decreasing the packed bed spacing has resulted in very small changes in the values of pressure drop, increasing it by less than 2% with Re ~ 8×10^4. When the fluid flow direction is reversed, considering a new particle packing structure, pressure drop values have changed in all the models showing that particles' orientation has a significant role in fluid hydraulic behavior. As the numerical showed, reversing the fluid flow could have a 13.5% increase in the air pressure drop determined in the model with 200 mm bed spacing, while decreasing the bed spacing to 150 mm and 100 mm eases the growth, respectively to 13 and 12%. Therefore, particle randomness is the dominant factor, affecting the pressure drop while bed spacing showed very small effects on the hydraulic behaviors of air passing through intermittent packed beds.

Figure 10 shows the heat convection coefficient calculated for various SAH-M3 configurations operating at Re ~ 8×10^4, where D indicates the direct flow and R represents reverse flow, imposed on 100, 150, and 200 mm spacing packed bed designs. One of the important points is that in all the tested models, as the air passes through the packed beds, h is increasing from the first to the second and third. Evaluating the effects of randomness, which means comparing the values in direct and reverse flows, it was revealed that the particles' orientations do not have a very large impact on the heat convection coefficient among all the packed beds, where this deviation revolves around ± 1%. Investigations for the packed-bed spacing also suggest that decreasing the length between each two consecutive packed beds could not affect the collector thermal performance significantly, where a very slight increase of 2 % might be seen when the values of PB3 are compared between the 200 and 100 mm spacing. Thus,

it can be concluded that the numerical result of this study has an acceptable accuracy to be used in further analyses regardless of the packed-bed spacing and particle randomness.

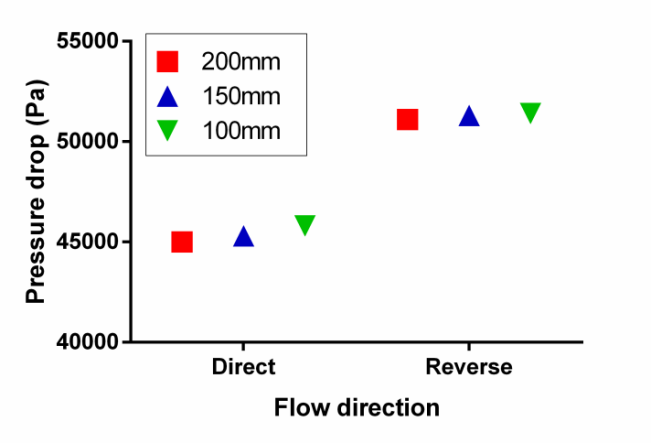

Fig. 9: Effects of flow direction (particle randomness) and bed spacing on the total pressure drop obtained along the solar collector at Re ~ 8 × 10^4.

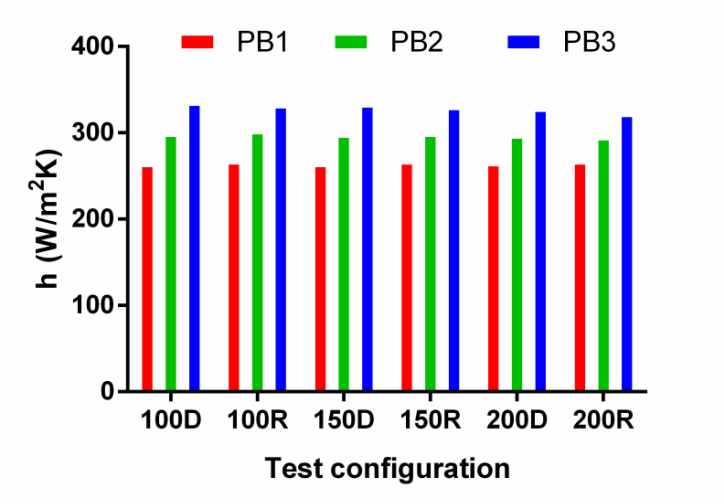

Fig. 10: The variation in heat transfer coefficient using various bed spacing and two different packing formations.

6. Conclusions

Several simulations were developed, using Star CCM+ software to study the airflow behavior inside a solar collector assisted with several intermittent packed beds at the pore scale. Reaching a good accuracy in the validation of numerical results with the general correlations, thermo-hydraulic behaviors of the collector were investigated, testing the number of packed beds and various air mass flow rates. The obtained results showed that the pressure drop could increase up to 1.15 bar when air with a mass flow rate of 0.08 kg/s passes through the three packed beds. However, the detailed analysis revealed that as the air passes through the second bed, it losses a fraction of its kinetic energy, leaving the third bed with a reduced pressure drop. The thermal results proved that the intermittent implementation of packed zones leads the heat transfer improvements at high Re, increasing the turbulent conditions in the fluid regime from one bed to the other. Thus, the values of the heat transfer coefficient rise by almost a factor of 2 for the packed bed number 1 and 3 at Re ~ 1.3 × 10^5. This enhancement suggested that at the highest airflow rate considered in this study, it is boosted by the thermal mixing that occurred in the porous structure of the beds. Finally, the sensitivity study showed that the thermal performance of the proposed solar collector has the least dependency on the parameters such as particles' orientation and bed spacing with only 2%, while hydraulic results may alter up to 13.5% if the packing structure differs.

7. Acknowledgments

We acknowledge the use of the computational resources provided by hpc@polito, which is a project of Academic Computing within the Department of Control and Computer Engineering at the Politecnico di Torino (http://hpc.polito.it). This work has also been supported by Italian Super Computing Resource Allocation (ISCRA-CINECA) within the Application ID: GRECIAN – HP10C6U7V4.

8. References

Allio, A., Difonzo, R., Leggieri, A., Legrand, F., Marchesin, R., Savoldi, L., 2020. Test and Modeling of the Hydraulic Performance of High-Efficiency Cooling Configurations for Gyrotron Resonance Cavities. Energies.

Azad, R., Bhuvad, S., Lanjewar, A., 2021. Study of solar air heater with discrete arc ribs geometry: Experimental and numerical approach. Int. J. Therm. Sci. 167, 107013.

Bellos, E., Tzivanidis, C., 2018. Investigation of a star flow insert in a parabolic trough solar collector. Appl. Energy 224, 86–102.

Bellos, E., Tzivanidis, C., Tsimpoukis, D., 2017. Thermal enhancement of parabolic trough collector with internally finned absorbers. Sol. Energy 157, 514–531.

Bensaci, C.-E., Moummi, A., Sanchez de la Flor, F.J., Rodriguez Jara, E.A., Rincon-Casado, A., Ruiz-Pardo, A., 2020. Numerical and experimental study of the heat transfer and hydraulic performance of solar air heaters with different baffle positions. Renew. Energy 155, 1231–1244.

Choudhury, C., Chauhan, P.M., Garg, H.P., 1995. Economic design of a rock bed storage device for storing solar thermal energy. Sol. Energy 55, 29–37.

Chouksey, V.K., Sharma, S.P., 2016. Investigations on thermal performance characteristics of wire screen packed bed solar air heater. Sol. Energy 132, 591–605.

Dhiman, P., Thakur, N.S., Kumar, A., Singh, S., 2011. An analytical model to predict the thermal performance of a novel parallel flow packed bed solar air heater. Appl. Energy 88, 2157–2167.

Dixon, A.G., Walls, G., Stanness, H., Nijemeisland, M., Stitt, E.H., 2012. Experimental validation of high Reynolds number CFD simulations of heat transfer in a pilot-scale fixed bed tube. Chem. Eng. J. 200–202, 344–356.

Dong, Y., Sosna, B., Korup, O., Rosowski, F., Horn, R., 2017. Investigation of radial heat transfer in a fixed-bed reactor: CFD simulations and profile measurements. Chem. Eng. J. 317, 204–214.

Ebadi, H., Allio, A., Cammi, A., Savoldi, L., 2021. First numerical evaluation of the thermal performance of a tubular receiver equipped with Raschig rings for CSP applications, in: Power 2021. ASME.

Gorjian, S., Ebadi, H., Calise, F., Shukla, A., Ingrao, C., 2020. A review on recent advancements in performance enhancement techniques for low-temperature solar collectors. Energy Convers. Manag. 222, 113246.

Kumar, A., Kim, M.H., 2017. Solar air-heating system with packed-bed energy-storage systems. Renew. Sustain. Energy Rev. 72, 215–227.

Kumar, B.N., Reddy, K.S., 2020. Numerical investigations on metal foam inserted solar parabolic trough DSG absorber tube for mitigating thermal gradients and enhancing heat transfer. Appl. Therm. Eng. 178, 115511.

Moghaddam, E.M., Foumeny, E.A., Stankiewicz, A.I., Padding, J.T., 2021. Heat transfer from wall to dense packing structures of spheres, cylinders and Raschig rings. Chem. Eng. J. 407, 127994.

Mwesigye, A., Bello-Ochende, T., Meyer, J.P., 2014. Heat transfer and thermodynamic performance of a parabolic trough receiver with centrally placed perforated plate inserts. Appl. Energy 136, 989–1003.

Prasad, S.B., Saini, J.S., Singh, K.M., 2009. Investigation of heat transfer and friction characteristics of packed bed solar air heater using wire mesh as packing material. Sol. Energy 83, 773–783.

Raj, A.K., Srinivas, M., Jayaraj, S., 2019. A cost-effective method to improve the performance of solar air heaters using discrete macro-encapsulated PCM capsules for drying applications. Appl. Therm. Eng. 146, 910–920.

Ramadan, M.R.I., El-Sebaii, A.A., Aboul-Enein, S., El-Bialy, E., 2007. Thermal performance of a packed bed double-pass solar air heater. Energy 32, 1524–1535.

Savoldi, L., Allio, A., Bovento, A., Cantone, M., Fernandez Reche, J., 2020. Experimental and numerical investigation of a porous receiver equipped with Raschig Rings for CSP applications. Sol. Energy.

Shih, T.-H., Liou, W.W., Shabbir, A., Yang, Z., Zhu, J., 1995. A new k-ϵ eddy viscosity model for high reynolds number turbulent flows. Comput. Fluids 24, 227–238.

Singh, H., Saini, R.P., Saini, J.S., 2013. Performance of a packed bed solar energy storage system having large sized elements with low void fraction. Sol. Energy 87, 22–34.

Soe, T.M., Khaing, S.Y., 2017. Comparison of Turbulence Models for Computational Fluid Dynamics Simulation of Wind Flow on Cluster of Buildings in MandalayNo Title. Int. J. Sci. Res. Publ. 7, 337–350.

Yılmaz, İ.H., Mwesigye, A., Göksu, T.T., 2020. Enhancing the overall thermal performance of a large aperture parabolic trough solar collector using wire coil inserts. Sustain. Energy Technol. Assessments 39, 100696.